Hydrothermal Syntheses, Structural Characterizations, and Photoluminescence Properties of Three Fluorinated Indium Phosphates with Bipyridyl Ligands: $In_3F_2(2,2'\text{-bipy})_2(HPO_4)_2(H_{1.5}PO_4)_2$, $In_2F_2(H_2O)(2,2'\text{-bipy})(HPO_4)_2$, and $In_2F_2(H_2O)(2,2'\text{-bipy-5-amine})(HPO_4)_2$

Chao Chen,[†,‡] Yunling Liu,[†] Shuhua Wang,[‡] Guanghua Li,[†] Minghui Bi,[†] Zhuo Yi,[†] and Wenqin Pang*[,†]

State Key Laboratory of Inorganic Synthesis and Preparative Chemistry, College of Chemistry, Jilin University, Changchun 130012, P. R. China, and Institute of Miniature Analytical Instrumentation, College of Chemistry, Jilin University, Jilin Province Research Center for Engineering and Technology of Spectral Instruments, Changchun 130023, P. R. China

Received October 31, 2005. Revised Manuscript Received April 23, 2006

Three novel fluorinated indium phosphates with the formulas $In_3F_2(2,2'\text{-bipy})_2(HPO_4)_2(H_{1.5}PO_4)_2$ (**1**), $In_2F_2(H_2O)(2,2'\text{-bipy})(HPO_4)_2$ (**2**), and $In_2F_2(H_2O)(2,2'\text{-bipy-5-amine})(HPO_4)_2$ (**3**) have been prepared hydrothermally in the presence of 2,2′-bipy and 2,2′-bipy-5-amine ligands. Single-crystal X-ray diffraction analysis reveals that **1** possesses an unusual neutral chained structure, which is not only the first 1D chain in the indiumphosphate family but also shows a new type of chain structure compared with those metalphosphates reported in the literature. Meanwhile, **2** and **3** present 2D undulated sheetlike structures with the same inorganic framework topology. The adjacent layers are stably packed together and exhibit interesting 3D supramolecular arrays with $\pi-\pi$ interactions of the bipy groups. It is noteworthy that the different ratios of In:P for reactant addition lead to the formation of different structures in the presence of the same bipy ligands (In:P = 1:6 for compound **1** and In:P =1:4 for **2**). By comparatively studying the photoluminescence properties of these compounds, we may conclude that the photoluminescence originates from ligand-centered $\pi-\pi^*$ transitions. The as-synthesized products are further characterized by powder X-ray diffraction, thermogravimetric analysis, ^{31}P MAS NMR and IR spectroscopy, ICP, and elemental analysis.

Introduction

In materials science, metal phosphates, with either an inorganic or a hybrid organic−inorganic framework, have been of great interest in the past few years because of their potential applications in catalysis and separation processes, and also because of the fascinating structural features exhibited by them.[1,2] Frequent use of hydrothermal (solvothermal) technology and the influence of organic amines on inorganic frameworks promote the formation and structural diversity of the metal phosphates. In addition, the presence of fluoride as a mineralizer in hydrothermal synthesis frequently has a pronounced effect on the solid-state phases produced and may even result in the incorporation of fluoride into the inorganic framework.[3] One approach to designing and synthesizing novel materials in this system employs organic amines as structure-directing agents (SDA) or templates. An alternative path to this method uses the organic component as ligand, which can be directly coordinated to the metal phosphate scaffolding to form organic−inorganic hybrid metal phosphates.[4] Using these two approaches, a rich structural chemistry has already been established for group 13 phosphates of Al[5,6] and Ga,[7] and work is now emerging on the indium phosphate family. So far, there are three-dimensional open framework InPOs with In:P ratios of 1:2,[8,9] 2:3,[10] 1:1,[11,12] 9:8,[13] 5:4,[14] and 6.8:8[15] and 2D layered

* To whom correspondence should be addressed. Fax: 86-431-5168624. E-mail: wqpang@mail.jlu.edu.cn.

† State Key Laboratory of Inorganic Synthesis and Preparative Chemistry, Jilin University.

‡ Institute of Miniature Analytical Instrumentation, Jilin University.

(1) Cheetham, A. K.; Férey, G.; Loiseau, T. *Angew. Chem., Int. Ed.* **1999**, *38*, 3268 and references therein.
(2) Feng, S.; Xu, R. *Acc. Chem. Res.* **2001**, *34*, 239.
(3) (a) Kessler, H. *Microporous Mesoporous Mater.* **1998**, *22*, 495. (b) Loiseau, T.; Férey, G. *J. Chem. Soc., Chem. Commun.* **1992**, 1197. (c) Paillaud, J. L.; Marler B.; Kessler, H. *J. Chem. Soc., Chem. Commun.* **1996**, 1293.
(4) Hagrman, P. J.; Hagrman, D.; Zubieta, J. *Angew. Chem., Int. Ed.* **1999**, *38*, 2638 and references therein.
(5) Wilson, S. T.; Lok, B. M.; Flanigen, E. M. U.S. Patent 4 310 440, 1982.
(6) Huo, Q.; Xu, R. *J. Chem. Soc.* **1992**, 168.
(7) Esternam, M.; McCusker, L. B.; Baerlocher, C.; Merrouche, A.; Kessler, H. *Nature* **1991**, *352*, 320.
(8) Dhigra, S. S.; Haushalter, R. C. *J. Chem. Soc., Chem. Commun.* **1993**, 1665.
(9) Chen, C.; Yi, Z.; Ding, H.; Li, G.; Bi, M.; Yang, Y.; Li, S.; Li, W.; Pang, W. *Microporous Mesoporous Mater.* **2005**, *83*, 301.
(10) Dhingra, S.; Haushalter, R. *J. Solid State Chem.* **1994**, *112*, 96.
(11) Yi, Z.; Yang, Y.; Huang, K.; Li, G.; Chen, C.; Wang, W.; Liu, Y.; Pang, W. *J. Solid State Chem.* **2004**, *177*, 4073.
(12) Xu, Y.; Koh, L. L.; An, L. H.; Xu, R.; Qiu, S. *J. Solid State Chem.* **1995**, *117*, 373.
(13) Williams, I. D.; Yu, J.; Du, H.; Chen, J.; Pang, W. *Chem. Mater.* **1998**, *10*, 773.
(14) Du, H.; Chen, J.; Pang, W.; Yu, J.; Williams, I. D. *Chem. Commun.* **1997**, 781.

10.1021/cm052395x CCC: $33.50
Published on Web 05/28/2006

Table 1. Crystal Data and Structure Refinement for 1−3

	1	2	3
empirical formula	$C_{20}H_{21}F_2In_3N_2O_{16}P_4$	$C_{10}H_{12}F_2In_2N_2O_9P_2$	$C_{10}H_{13}F_2In_2N_3O_9P_2$
fw	1079.75	633.80	648.81
cryst syst	triclinic	triclinic	triclinic
space group	$P\bar{1}$ (No. 2)	$P\bar{1}$ (No. 2)	$P\bar{1}$ (No. 2)
a (Å)	8.8932(11)	7.8843(17)	7.899(3)
b	9.0338(11)	10.321(2)	10.405(4)
c	10.6253(13)	11.395(2)	11.387(5)
α (deg)	72.445(2)	107.139(3)	α108.01(3)
β (deg)	75.252(2)	105.101(3)	104.52(3)
γ (deg)	74.819(2)	99.328(3)	99.36(2)
V (Å^3)	771.04(16)	826.3(3)	831.9(6)
Z	1	2	2
D_{calcd} (Mg/m^3)	2.325	2.547	2.590
abs coeff (mm^{-1})	5.051	3.059	3.043
F (000)	522	608	624
cryst size (mm^3)	0.249 × 0.107 × 0.102	0.116 × 0.086 × 0.049	0.102 × 0.071 × 0.050
θ range for data collection (deg)	2.05−28.60	1.98−28.47	1.99−28.23
limiting indices	$-11 \le h \le 11$, $-11 \le k \le 12$, $-7 \le l \le 13$	$-10 \le h \le 10$, $-13 \le k \le 13$, $-7 \le l \le 14$	$-10 \le h \le 9$, $-13 \le k \le 12$ $-8 \le l \le 15$
no. of reflns collected/unique	4825/3425 [*R*(int) = 0.0414]	5128/3650 [*R*(int) = 0.0452]	5845/4021 [*R*(int) = 0.0754]
data/restraints/params	3425/0/267	3650/0/276	4021/0/253
GOF on F^2	1.011	1.109	0.907
final R indices [$I > 2\sigma(I)$][a]	R_1= 0.0259, wR_2=0.0658	R_1=0.0446, wR_2=0.1038	R_1=0.0598, wR_2=0.1222
R indices (all data)	R_1=0.0284, wR_2=0.0676	R_1=0.0527, wR_2=0.1071	R_1=0.1094, wR_2=0.1397
largest diff. peak and hole (e Å^{-3})	1.232 and −0.727	1.318 and −0.862	1.855 and −2.523

[a] $R_1 = \sum||F_o| - |F_c||/\sum|F_o|$. $wR_2 = [\sum[\ w(F_o^2 - F_c^2)^2]/\sum[\ w(F_o^2)^2]]^{1/2}$.

structures with In:P ratios of 1:3,[16] 1:2,[17−19] 4:7,[20] and 1:1.[14] Furthermore, two indium phosphites have also been reported recently.[21,22] However, compared to the systematic, enormous exploitation of indium phosphates using organic amines as structure-directing agents and/or templates, reports on indium phosphates employing the organic amine as ligand are rarely documented.[17] Compared with inorganic ligands, organic multidentate ligands possess more rich coordination sites and a higher capacity of passivating metal sites by reducing the available metal ion binding sites, which may inhibit inorganic structure growth in certain directions.[23] One may expect that the rational design of crystalline solids with complex architectures may be realized through shrewd choice of organic species. Furthermore, the metal-coordination compounds with pyridine type ligands have received much attention recently because of their good performance in sensor technologies and luminescence devices.[24] These ideas have prompted us to choose indium as the metal ion, hydrofluoric acid as the mineralizer, and 2,2′-bipyridyl (2,2′-bipy) and its derivative 2,2′-bipyridine-5-amine (2,2′-bipy-5-amine) as organic ligands. Employing this strategy, we have successfully synthesized three novel fluorinated indiumphosphates, $In_3F_2(2,2'\text{-bipy})_2(HPO_4)_2(H_{1.5}PO_4)_2$ (**1**), $In_2F_2(H_2O)(2,2'\text{-bipy})(HPO_4)_2$ (**2**), and $In_2F_2(H_2O)(2,2'\text{-bipy-5-amine})(HPO_4)_2$ (**3**), which possess unusual neutral 1D chains and 2D undulated sheetlike structures with the same inorganic topology, respectively. Despite the fact that the inorganic frameworks of compounds **2** and **3** are similar, the different chromophores (ligands) of the two compounds lead to diverse luminescence properties. Herein, we comparatively report the syntheses, structures, and photoluminescence properties of these compounds.

Experimental Section

Synthesis. All reagents were of analytical grade. The three compounds were hydrothermally prepared from a starting mixture containing 2,2′-bipy (for compounds **1** and **2**) and 2,2′-bipy-5-amine (for compound **3**) as organic ligands. For **1** and **2**, indium nitrate ($In(NO_3)_3{\cdot}4.5H_2O$, 99.5%), phosphoric acid (85 wt %), 2,2′-bipy, hydrofluoric acid (40%; ***Caution****: toxic and highly irritating; work in a laboratory hood when handling concentrated HF*), and distilled water were mixed in a 1:6.0:2.0:5.0:250 molar ratio of $In(NO_3)_3{\cdot}4.5H_2O{:}H_3PO_4$:2,2′-bipy:HF:$H_2O$ and a 1:4.0:2.2:5.0:250 molar ratio of $In(NO_3)_3{\cdot}4.5H_2O{:}H_3PO_4$:2,2′-bipy:HF:$H_2O$, respectively. For **3**, indium nitrate, phosphoric acid, 2,2′-bipy-5-amine, hydrofluoric acid, and distilled water were mixed in a 1:4.0:2.5:5.0:250 molar ratio of $In(NO_3)_3{\cdot}4.5H_2O{:}H_3PO_4$:2,2′-bipy-5-amine:HF:$H_2O$. The mixture was sealed in a 15 mL Teflon-lined stainless steel autoclave with a filling capacity of ∼50% and heated at 180 °C for 8 days for **1** and 10 days for **2** and **3** under autogenous pressure. The resulting platelike colorless (**1** and **2**) and yellow (**3**) crystals were recovered by filtration, further washed thoroughly with distilled water, and dried at room temperature.

Characterization. Powder X-ray diffraction (XRD) data were collected on a Siemens D5005 diffractometer with Cu Kα radiation (λ = 1.5418 Å). The step size was 0.02° and the count time was 2 s. The elemental analyses were performed on a Perkin−Elmer 2400 LSII element analyzer. Inductively coupled plasma (ICP) analyses

(15) Thirumurugan, A.; Natarajan, S. *Dalton Trans.* **2003**, 3387.
(16) Chippindale, A.; Brech, S. *Chem. Commun.* **1996**, 2781.
(17) Lii, K.-H.; Huang, Y.-F. *Inorg. Chem.* **1999**, *38*, 1348.
(18) Yu, J.; Sung, H. H.-Y.; Williams, I. D. *J. Solid State Chem.* **1999**, *142*, 241.
(19) Du, Y.; Yu, J.; Wang, Y.; Pan, Q.; Zou, Y.; Xu, R. *J. Solid State Chem.* **2004**, *177*, 3032.
(20) Chippindale, A. M.; Brech, S. J.; Cowley, A. R.; Simpson, W. M. *Chem. Mater.* **1996**, *8*, 2259.
(21) Wang, L.; Shi, S.; Ye, J.; Fang, Q.; Fan, Y.; Li, D.; Xu, J.; Song, T. *Inorg. Chem. Commun.* **2005**, *8*, 271.
(22) Yi, Z.; Chen, C.; Li, S.; Li, G.; Meng, H.; Cui, Y.; Yang, Y.; Pang, W. *Inorg. Chem. Commun.* **2005**, *8*, 166.
(23) Plater, M. J.; Foreman, M. R. S.; Coronado, E.; Gümez-García, C. J.; Slawin, A. M. Z. *J. Chem. Soc., Dalton Trans.* **1999**, *23*, 4209.
(24) (a) Balzani, V.; Juris, A.; Venturi, M.; Campagna, S. *Chem. Rev.* **1996**, *96*, 759. (b) Lin, Z. Z.; Jiang, F. L.; Chen, L.; Yuan, D. Q.; Hong, M. C. *Inorg. Chem.* **2005**, *44*, 73. (c) Lin, Z. E.; Zhang, J.; Zheng, S. T., Yang, G. Y. *Microporous Mesoporous Mater.* **2004**, *68*, 65.

were carried out on a Perkin−Elmer Optima 3300 DV ICP instrument. The infrared (IR) spectra were recorded within the 400−4000 cm^{-1} region on a Nicolet Impact 410 FTIR spectrometer using KBr pellets. A Perkin−Elmer TGA 7 thermogravimetric analyzer was used to obtain thermogravimetric analysis (TGA) curves in an atmospheric environment with a heating ratio of 10 °C min^{-1}. The ^{31}P MAS NMR spectra were acquired at a ^{31}P frequency of 161.81 MHz on an Infinity Plus spectrometer. The ^{31}P chemical shifts were reported relative to 85% H_3PO_4 as an external reference. Fluorescence spectra were measured on a Perkin−Elmer LS 55 luminescence spectrometer, equipped with a 450 W xenon lamp.

Determination of Crystal Structures. A suitable single crystal was selected for single-crystal XRD analysis. The data were collected on a Bruker Smart CCD diffractometer (λ (Mo Kα) = 0.71073 Å) at 20 ± 2 °C. A total of 4825 reflections for compound **1**, 5128 reflections for **2**, and 5845 reflections for **3** were collected, with 3425, 3650, and 4021 unique reflections, respectively ($R_{int\ 1}$ = 0.0414, $R_{int\ 2}$ = 0.0452, and $R_{int\ 3}$ = 0.0754). Data processing was accomplished with the Process-Auto processing program. The structures of the three compounds were all solved by heavy-atom methods and refined by a full-matrix least-squares approach on F^2 using the SHELXTL 5.1 software package.[25] The In and P atoms were located first, and then the O, F, C, and N atoms were found in the final difference Fourier maps. The hydrogen atoms of the framework were initially located from difference Fourier maps and for the final refinement were placed geometrically except for those of compound **1**. Finally, the non-hydrogen atoms were all refined anisotropically. The detailed crystallographic data of the three compounds are listed in Table 1.

Results and Discussion

Description of the Structures. The final atomic coordinates with isotropic temperature factors for the three compounds are listed in Tables 2−4 of the Supporting Information, whereas selected bond lengths and angles are presented in Tables 5−7 of the Supporting Information.

Single-crystal X-ray diffraction analysis reveals that the unit cell of compound **1** contains two crystallographically distinct In atoms; one (In(1)) resides on the 2-fold symmetry axis, the other unique In (In(2)) atom in the general position, and two P atoms are also located on the general positions (Figure 1a). Each In atom is octahedrally coordinated, but the coordination environments are different. In(1) shares four vertex oxygen atoms with adjacent P atoms (In−O_{av} = 2.110 Å) and two bridging F atoms with In(2) atoms (In−F_{av} = 2.107 Å). Interestingly, the F(1)−In(1)−F(1A) bond angle for two fluorine atoms, O(5)−In(1)−O(5A) and O(7)−In(1)−O(7A) for oxygen atoms in a trans position are all exactly 180°, which is rarely documented in octahedral indium phosphates. Except for the bridging fluorine atom shared with the In(1) atom, the In(2) atom is coordinated by two nitrogen atoms from a 2,2′-bipy ligand and three oxygen atoms with adjacent P atoms. The In−O/N/F bond distances are in the expected range of 2.080(2)−2.272(2) Å (In(2)−F = 2.141(2) Å, In(2)−O_{av} = 2.095 Å, and In(2)−N_{av} =2.262 Å). The tetrahedral P(2) atom shares three oxygen atoms with adjacent In atoms, leaving the other oxygen atom as a terminal P−OH group, with P−O bond lengths of 1.559(3) Å. The P(1) atom is unusually present as a $H_{1.5}PO_4$ group. It shares two oxygen atoms with adjacent In atoms, leaving the other two as terminal oxygen atoms. The bond length of P(1)−O(2) is 1.574(3) Å, which should be attributed to the P−OH bond, inevitably. However, the P(1)−O(3) bond length is 1.532(2) Å, slightly shorter than the terminal P−OH

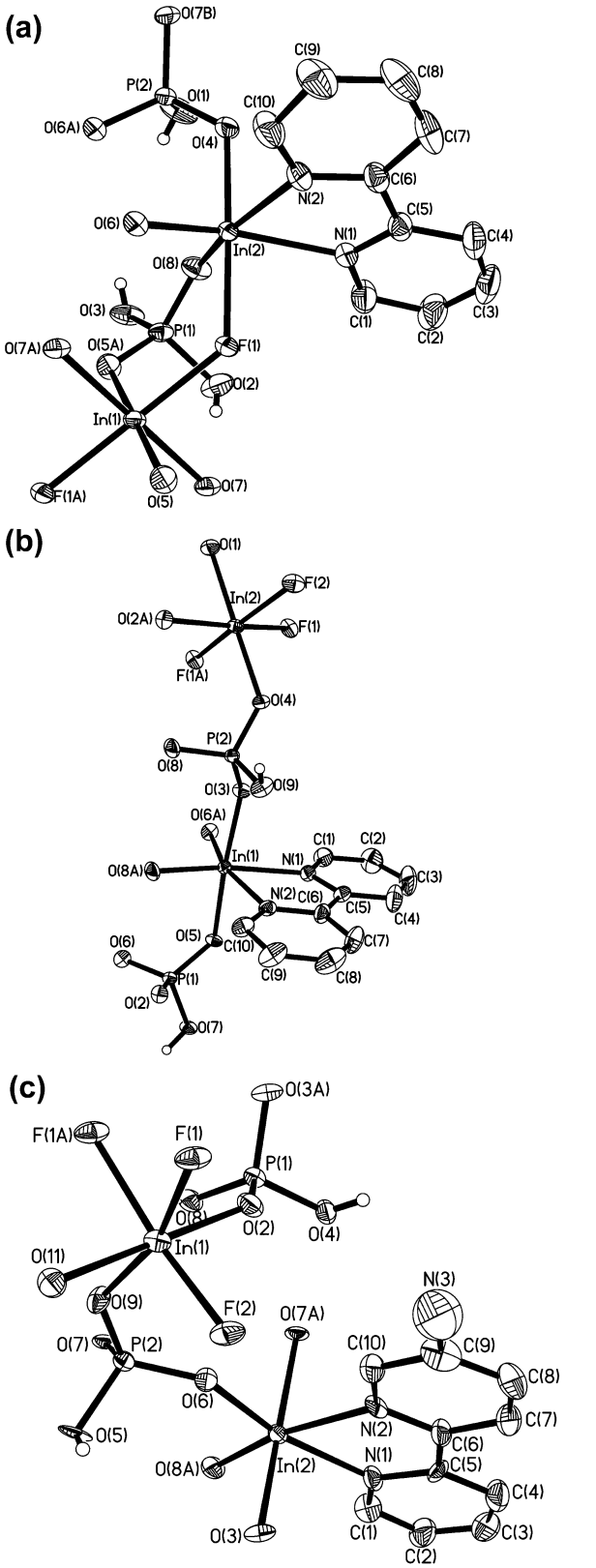

Figure 1. Asymmetric units of **1**, **2**, and **3** (thermal ellipsoids at the 50% probability level).

(25) *SMART* and *SAINT* (software packages); Siemens Analytical X-ray Instruments Inc.: Madison, WI, 1996.

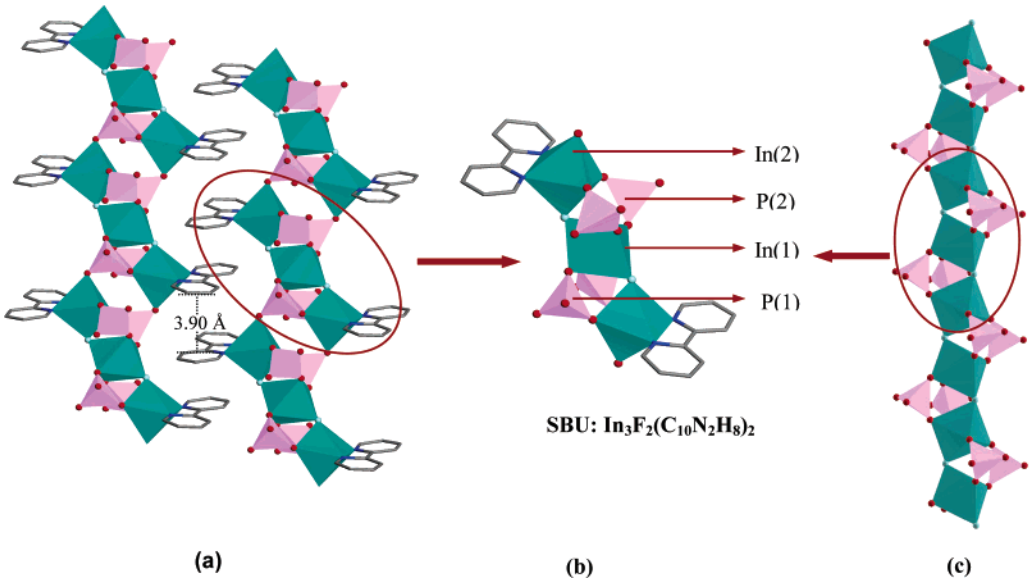

Figure 2. (a) Polyhedral representation of the chain structure along the *a* axis for **1**. (b) Note the unusual SBU, the heptamer $In_3F_2(bipy)_2(HPO_4)_3(H_2PO_4)$, constructing into the neutral chains. (c) Infinite chain in tancoite.

bond and longer than the terminal P═O bond, and is assumed to be scrambling/disorder of P−O⁻/P═O functionalities. In fact, the H peak of electron density is found between the two O(3) atoms and is shared by two $H_{1.5}P(1)O_4$ groups on the adjacent chains, the site occupation factor (SOF) of which is 0.5 for charge balance. Similar behavior has been observed in ZrPOs and GaPOs families.[26] Bond valence calculations for all atoms within the framework atoms for **1** are listed in Table 5 of the Supporting Information and confirm the valence assignment.[27]

The structure of **1** consists of infinite neutral chains, which may be understood in terms of an unusual secondary building unit (SBU), the heptamer, with a formula of $In_3F_2(bipy)_2(HPO_4)_3(H_2PO_4)$, built from four PO_4 (HPO_4, H_2PO_4) tetrahedra, two $In(2)FO_3N_2$ octahedra, and one central $In(1)F_2O_4$ octahedron, as shown in panels a and b of Figure 2. The $InFO_3N_2$ and InF_2O_4 octahedra are linked together by the bridging fluorine atoms in trans position to form a trimer, $In_3F_2O_{10}N_4$. Four PO_4 tetrahedra then cap the trimer by the bridging oxygen atoms to generate the heptamer. These heptamers further fuse together via vertex O(4) of the $HP(2)O_4$ group to construct the infinite neutral chain along the *a* axis. The two pyridine rings in the 2,2′-bipy molecule decorating the chain are almost coplanar with a dihedral angle of about 7.66°, and both rings are roughly perpendicular to the chain. Neighboring 2,2′-bipy ligands from two adjacent chains have a structure of offset parallel stacking and are separated by 3.9 Å, indicating significant attractive intermolecular aromatic interaction.[28] Thus, indium phosphate chains are extended into a three-dimensional supramolecular array via $\pi-\pi$ stacking interactions of the 2,2′-bipy ligands. In addition, the weak intra-/interchain hydrogen bonding interactions with an OH···O separation of 1.993−2.193 Å also perform a certain function on stabilizing the structure of **1**.

To the best of our knowledge, compound **1** is unusual in that it is not only the first 1D chain of the indiumphosphate family but also shows a new type of chain structure in metallophosphates (compared with those reported in the literature). Even though the SBU of the chain is observed in some tancoite-like compounds[29] (Figure 2c), the linked fashion is different between the two chains. For tancoite-like compounds, the chain is built from a central core constituted by a string of metal octahedra linked by their trans oxygen (or fluorine) apexes. However, for **1**, three indium octahedra are linked together by the bridging F atoms in trans position to form a trimer and then linked by PO_4 tetrahedra to generate an "interrupted tancoite" chain. The probable explanation is that the bipy ligands that exist in the reaction coordinate to all of the surplus In sites such that the steric hindrance of bipy groups decorating the chain prevents the indium molecules in the central core from linking to each other and forming a string structure.

Unlike compound **1** with a chained structure, compounds **2** and **3** are neutral layered networks with the same inorganic framework topology, the only difference of which is that the organic ligands of **2** are 2,2′-bipy, whereas that of **3** corresponds to 2,2′-bipy-5-amine. Here, we describe only the structure of compound **2** as a representative. Figure 1b shows the asymmetric unit of **2**. The structure consists of two independent In atoms and two phosphorus atoms. In(1) is coordinated by one bidentate 2,2′-bipy and four HPO_4 groups, whereas octahedral In(2) coordinates two bridging oxygen atoms with adjacent P atoms ($In(2)-O_{av} = 2.073$ Å) and two bridging F atoms with another In(1) atom, leaving the other ligands as a terminal F ($In(2)-F(2) = 2.071(4)$ Å)

(26) (a) Sung, H. H.-Y.; Yu, J.; Williams, I. D. *J. Solid State Chem.* **1998**, *140*, 46. (b) Chen, C. Y.; Lo, F. R.; Kao, H. M.; Lii, K. H. *Chem. Commun.* **2000**, 1061.
(27) (a) Brown, I. D.; Altermatt, D. *Acta Crystallogr., Sect. B* **1985**, *41*, 244. (b) Brese, N. E.; Keeffe, M. O. *Acta Crystallogr., Sect. B* **1991**, *47*, 192.
(28) Ferguson, S. B.; Sanford, E. M.; Seward, E. M.; Diederich, F. *J. Am. Chem. Soc.* **1991**, *113*, 5410.
(29) (a) Frank, C. H. *Acta Crystallogr., Sect. B* **1994**, *50*, 481. (b) Richard, I. W.; Franck, M.; Dermot, O. *Chem. Mater.* **2000**, *12*, 1977. (c) Zoe, A. D. L.; Philip, L.; Russell, E. M.; David, S. W.; Paul, A. W. *J. Solid State Chem.* **1999**, *142*, 455.

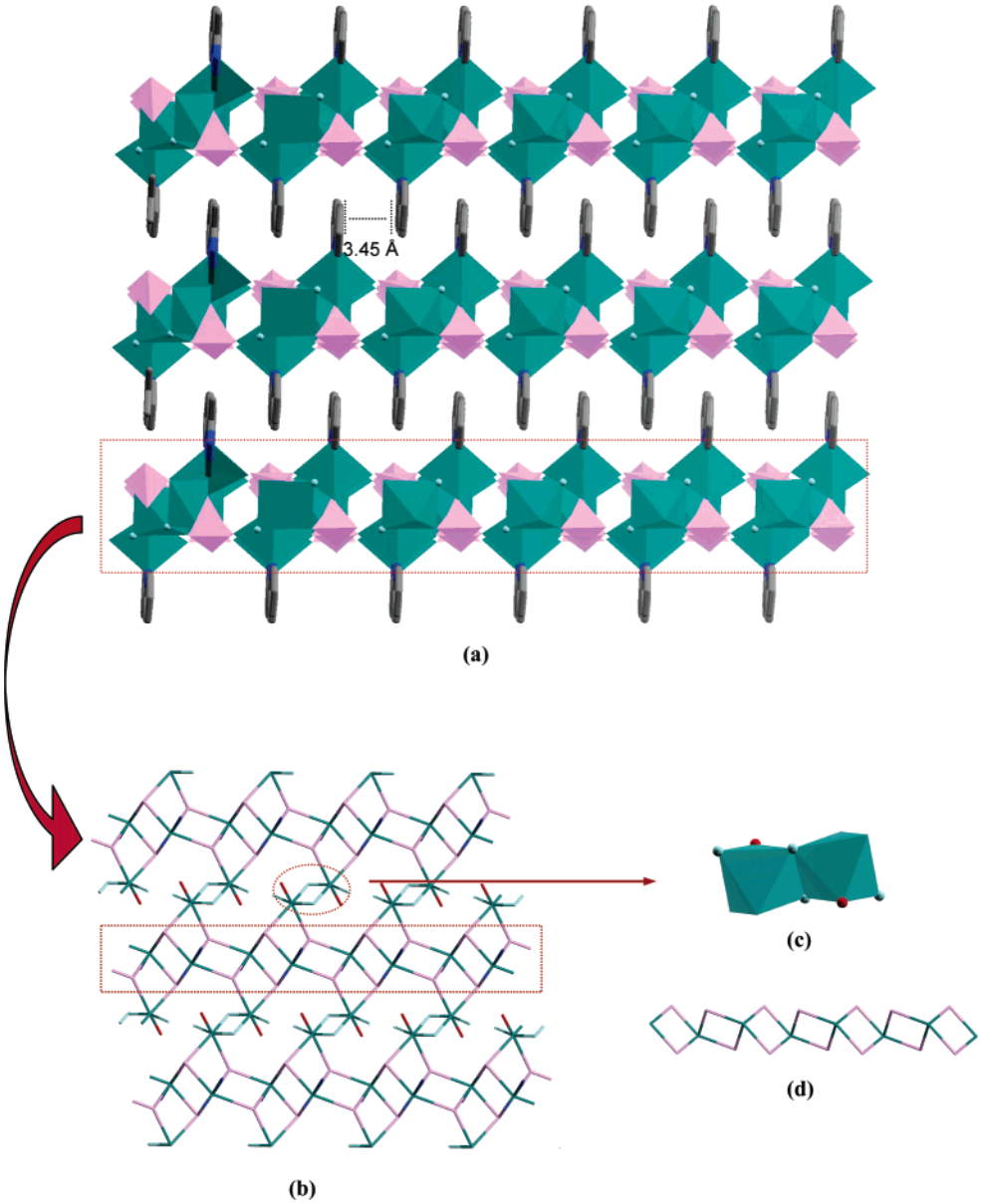

Figure 3. Description of the structural fashion of **2**. (a) Intercalation of the layers into a three-dimensional supramolecular array via the lateral bipy groups (perspective view along the [110] direction). (b) Stick view of the inorganic layer of **2** along the *z* axis (the bridging oxygen atoms and carbon atoms are omitted for clarity). (c) Unique edge-sharing dimer, $In_2O_6F_4$. (d) Corner-sharing-corner chain (CSC chain).

and a water molecule (In(2)−O(1) = 2.205(5) Å). All the coordination tetrahedra around the P atoms have some deformation because of the presence of an OH group. They link through oxygen to three adjacent indium atoms (P(1)−O_{av} = 1.521 Å and P(2)−O_{av} = 1.518 Å), with the fourth coordination site in each case corresponding to a terminal P−OH group, as shown by the longer P−O distances (P(1)−O(7) = 1.573(5) Å and P(2)−O(9) = 1.570(5) Å). These results are close to those observed previously in indium phosphates; bond valence calculations for all atoms within the framework atoms are listed in Table 6 of the Supporting Information.[8−20]

The polyhedral representation of structure **2** viewed down the [110] direction is shown in Figure 3a. It consists of a puckered inorganic indium phosphate layer staking in an AAAA fashion; organic 2,2′-bipy ligands decorate the inorganic layer and project above and below into the interlamellar regions. Neighboring 2,2′-bipy ligands from two adjacent layers are almost parallel to each other; there are possible $\pi-\pi$ interactions between them, as reflected in an average distance of 3.45 Å. It should be noted that there is H-bonding between adjacent layers, which performs a certain function on stabilizing the structure of **2**. The stick representation of the inorganic layer of **2** along the *z* axis is shown in Figure 3b. It is helpful to view this layer as being built from an infinite 1D chain and a dimer, as shown in panels c and d of Figure 3. First, a four-membered ring (4-MR), $In_2P_2O_4$, is formed from two InO_4N_2 and two HPO_4 groups via a corner-sharing mode. The 4-MRs then fuse together through their vertexes to form a classical corner-sharing-corner chain (CSC chain).[30] Finally, through P sites, the CSC chains link with a unique edge-sharing dimer, $In_2O_6F_4$, giving rise to a 4,10-membered ring undulating net structure. The dimer, which has not been observed in indiumphosphates

(30) Yu, J.; Xu, R. *Acc. Chem. Res.* **2003**, *36*, 481.

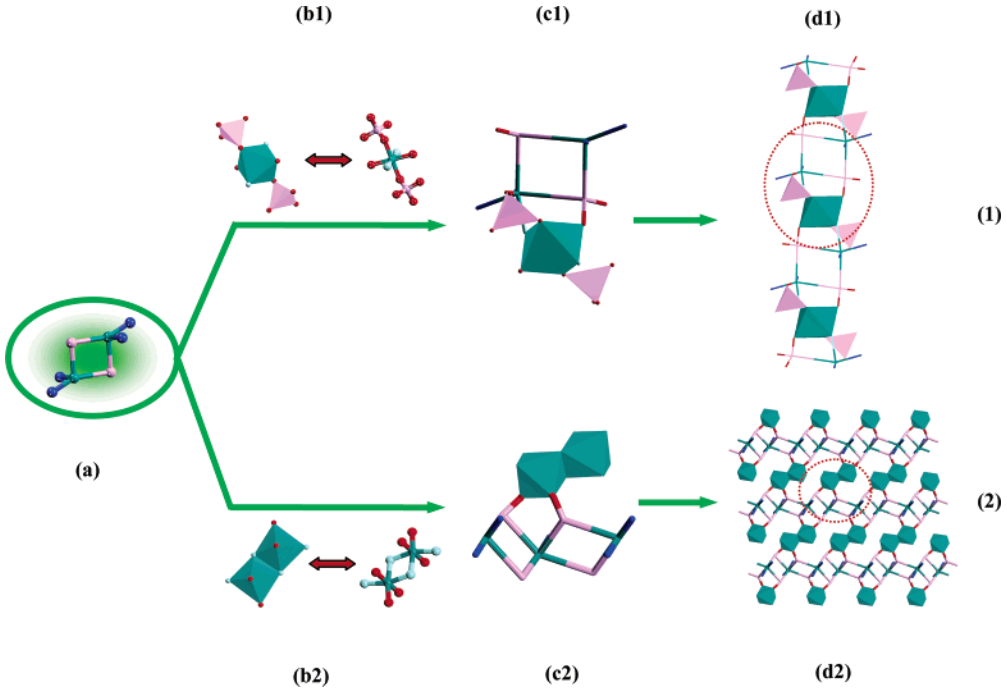

Figure 4. Building-up description of the influence of the In:P ratio on the structure. (a) Corner-shared four-membered ring, $In_2P_2O_4N_2$. (b1) Trimer of $InP_2F_2O_{10}$. (c1) Building block constructing into the chains of **1**. Note that the bridging F atoms are in trans positions. (d1) Representation for the structure of **1**. (b2) Edge-sharing dimer, $In_2O_6F_4$. Note that the bridging F atoms are in cis positions. (c2) Building block constructed into a layer of **2**. (d2) Representation for the structure of **2**.

before (but a similar edge-sharing octahedral dimer has been observed in the fluorinated iron (gallium) phosphate systems[31]), consists of four bridging O atoms with adjacent P atoms, two terminal F atoms, a terminal molecular water projecting into the 10-MR, and two bridging F atoms in cis position.

Influence of the In:P Ratio on the Structure. Interestingly, different In:P ratios for the reactant addition lead to the formation of different structures (In:P = 1:6 for structure **1** and In:P = 1:4 for **2**). To understand the relationship between the structure and the role of the In:P ratio, we give a building-up hypothesis in terms of a corner-shared four-membered ring, $In_2P_2O_4N_2$, presenting in the structure of both compounds, and the coordinate environment of In octahedra in the solution. In the case of the In−H_3PO_4−2,2′-bipy−HF−H_2O synthesis system, the $In_2P_2O_4N_2$ 4-MRs, as shown in Figure 4a, is a common motif in this system and is always formed initially. With different ratios of In:P for reactant addition, different coordinate environments of In octahedra forms in the solution. For compound **1**, an amount of phosphate groups coordinate to the octahedral In atoms, forming the trimers as shown in part b1 of Figure 4, progressively condensing with the 4-MRs through phosphate bridges and F bridges in trans positions to construct the chained structure (parts c1 and d1 of Figure 4). With an increasing In:P ratio, the In source is dominant in the reaction solution and a great quantity of In octahedra coordinate to each other through the F bridges in cis positions to form edge-sharing dimers, $In_2O_6F_4$, as shown in part b2 of Figure 4. Subsequently, the initial 4-MRs and the dimer fuse together through P sites to form the building block presented in part c2 of Figure 4. Finally, the building blocks construct the two-dimensional network of compound **2**.

Characterization. The ICP and elemental analysis results are in good agreement with the values from the single-crystal structure analysis. Calcd for **1** (wt %): In, 31.90; P, 11.47; C, 22.25; N, 5.189. Found: In, 32.25; P, 11.49; C, 24.13; N, 5.26. Calcd for **2** (wt %): In, 36.23; P, 9.77; C, 18.95; N, 4.42. Found: In, 37.18; P, 10.55; C, 17.25; N, 4.76. Calcd for **3** (wt %): In, 35.39; P, 9.55; C, 18.51; N, 6.48. Found: In, 36.45; P, 10.32; C, 19.86; N, 6.97.

The powder X-ray diffraction patterns for the three compounds are entirely consistent with that simulated on the basis of the single-crystal structure (Figure 5). The diffraction peaks on both patterns correspond well in position, indicating the phase purity of the as-synthesized samples. Some difference in reflection intensities between the simulated and experimental patterns is due to the variation in crystal orientation for the powder samples.

The thermogravimetric analysis curves of the three compounds show that the composition of **1** remained stable up to 350 °C. On further heating, a two-step weigh loss was observed. The initial weight loss between 350 and 650 °C should correspond to the departure of 2,2′-bipy ligands. However, the observed weight loss (24.15%) was much lower than the expected value (calcd: 28.93%). The lower reduction in this stage was due to the retention of carbon in the solid residue (black in color). The same phenomenon was observed in a GaPOs system.[32] The second step, occurring between 650 and 900 °C with a weight loss of 7.97%, should be attributed to the removal of HF, hydroxyls, and carbon from the black solid residue. The total observed weight loss (32.12%) for the two steps compared well with that calculated on the basis of the above interpretation. The XRD patterns of the post residue corresponded to dense

(31) Chang, W.; Chen, C.; Lii, K. H. *J. Solid State Chem.* **2003**, *172*, 6.

(32) Lin, Z.; Zhang, J.; Sun, Y.; Yang, G. *Inorg. Chem.* **2004**, *43*, 797.

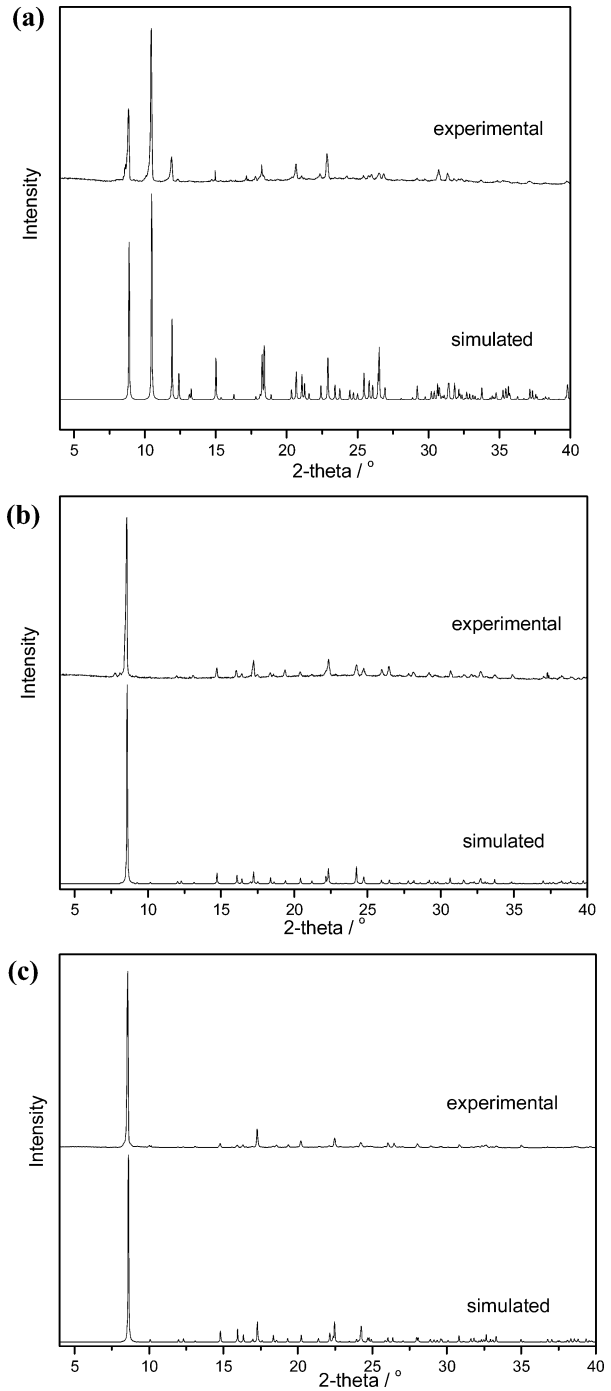

Figure 5. Experimental and simulated powder X-ray diffraction patterns of (a) **1**, (b) **2**, and (c) **3**.

$InPO_4$ (crystobalite form and JCPDS 08-0052) together with an amorphous phase. For **2** and **3**, the thermogravimetric analyses show that the weight loss of the compound is ca. 23.1% for **2** and 26.39% for **3** from 100 to 650 °C, corresponding to decomposition of the 2,2′-dipy (calcd: 24.61%) and 5-N-2,2′-dipy (calcd: 26.36%), respectively. A further weight loss of 10.18% for **2** and 9.24% for **3** at 650−850 °C is consistent with the removal of HF and molecular water from the compound. At that temperature, the compounds collapse and convert to an amorphous phase. At 900 °C, the amorphous phase recrystallizes to form an $InPO_4$ phase (JCPDS 08-0052), as confirmed by powder X-ray diffraction.

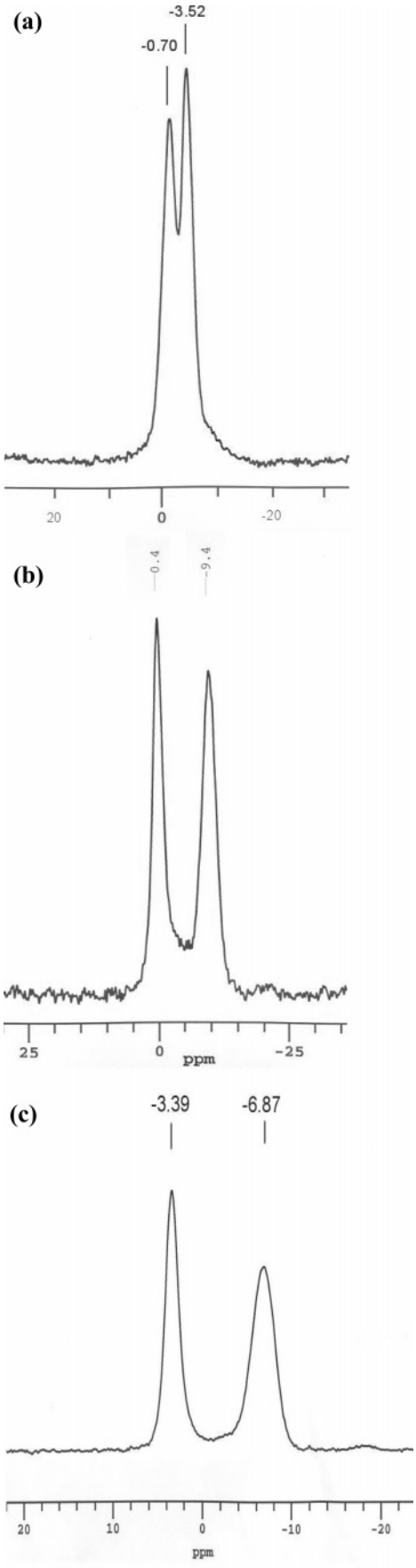

Figure 6. ^{31}P MAS NMR spectra for (a) **1**, (b) **2**, and (c) **3**.

^{31}P MAS NMR spectra of the as-synthesized compounds are shown in Figure 6. They show two signals at −0.70,

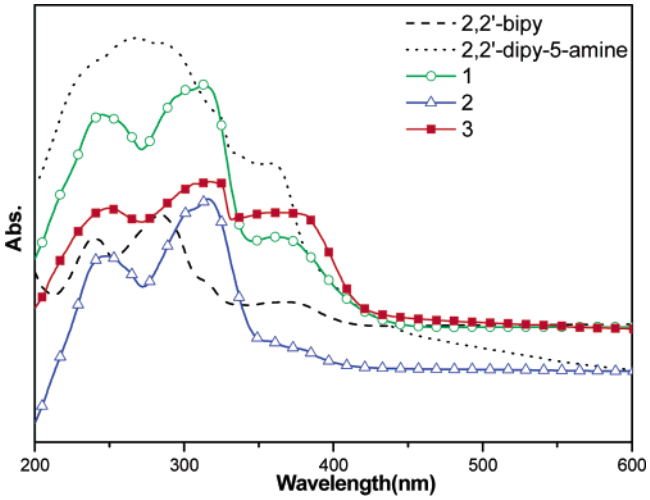

Figure 7. UV−vis absorption spectra of ligands 2,2′-bipy and 2,2′-bipy-5-amine and compounds **1**−**3**.

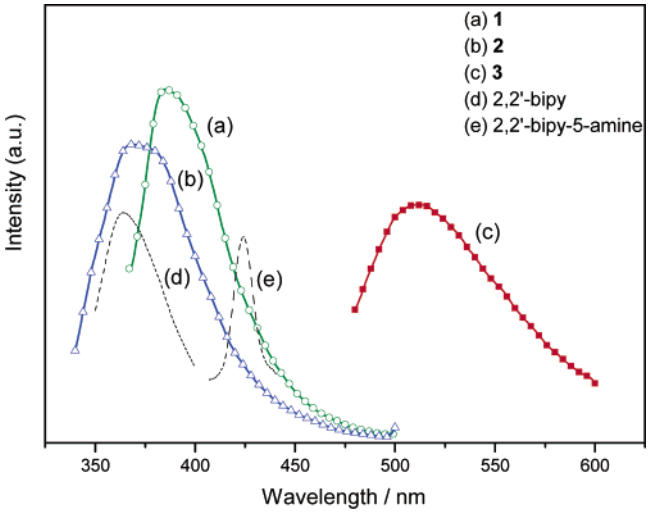

Figure 8. Solid-state fluorescence spectra at room temperature for three compounds and ligands: (a) **1**, (b) **2**, (c) **3**, (d) 2,2′-bipy, and (e) 2,2′-bipy-5-amine.

−3.52; −0.40, −9.40; and −3.39, −6.87 ppm, respectively, for **1**−**3**, with an intensity ratio of about 1:1. On the basis of the previous studies in phosphates,[19,33] we assigned the NMR peak at −0.70 ppm to the H_2PO_4 group and the other peaks to the HPO_4 groups. The ^{31}P signals of the three compounds are in agreement with the crystallographically distinct P sites in the structure and are characteristic for the tetrahedral phosphate sites.

The IR spectrum of **1** showed broad bands at 3135 and 3067 cm^{-1}, corresponding to the stretching vibrations of C−H and N−H bonds. The sharp peaks at 1611, 1563, 1483, 1437, and 1322 cm^{-1} were assigned to the bipyridyl ring stretching vibrations. The broad bands at 1052 and 929 cm^{-1} were associated with the asymmetric stretching vibrations of In−O and P−O bonds. The absorption at 530 and 485 cm^{-1} appeared as well, which may be due to bending vibrations of phosphate groups. The absorption bands appeared at 3124, 3079, 1605, 1573, 1470, 1440, 1322, 1203, 1108, 1073, 1031, 915, 859, 776, and 520 cm^{-1} for **2**; the bands appeared at 3372, 3121, 3079, 1603, 1598, 1472, 1440, 1108, 1066, 1024, 915, and 509 cm^{-1} for **3**, which included characteristic bands of pyridyl rings, phosphate groups, and In−O bonds. The assignment of these bands is similar to that for compound **1**.

Luminescence Properties. Having the same organic ligand but different inorganic frameworks (compound **1** and **2**) or the same inorganic framework but different organic ligands (**2** and **3**) leads to the diverse photoluminescence properties. The UV−vis absorption spectra of the three compounds and organic ligands are shown in Figure 7. On the basis of the absorption spectra of the free ligands as well as those of the closely related title compounds, we assigned the dominant absorption bands in the 220−400 nm region to the intraligand $\pi-\pi^*$ transition of the bipy unit. The absorption spectra of the three compounds are red-shifted relative to the ligands, which may be due to perturbation of the $\pi-\pi^*$ transition of the bipy ligands by the metal atom.[34]

Figure 8 presents the emission spectra of the title compounds in the solid state at room temperature, together with those for ligands 2,2′-bipy and 2,2′-bipy-5-amine. When illuminated with a wavelength of 352 nm, **1** displays a strong fluorescence emission band centered at 385 nm, whereas **2** presents an emission band at 368 nm (λ_{ex} = 327 nm), blue-shifted in comparison to **1**. This may be due to the better overlap between adjacent bipy ligands of **1** compared to that of **2**, increasing the $\pi-\pi$ stacking interactions of **1** and leading to the red-shift phenomena.[35] For **3**, an emission band in the range of 480−590 nm (λ_{ex} = 463 nm) is observed, dramatically red-shifted compared to that of **2**, despite having the same inorganic framework. The probable explanation is that the conjugate effect of the asymmetrical amine to the bipy rings in 2,2′-bipy-5-amine molecules leads to this red-shift phenomena. Because the title compounds are thermally stable and insoluble in common polar and nonpolar solvents, they might be promising candidates for further application as blue- or green-light emitting materials.

Conclusion

Employing 2,2′-bipy and 2,2′-bipy-5-amine as organic ligands, three novel fluorinated indium phosphates with neutral frameworks have been synthesized hydrothermally. Their fascinating structure and synthesis conditions were compared, a possible relationship between the structure and In:P ratio for the reactant addition were discussed. Importantly, comparison of the photoluminescence properties of the three compounds presents some distinct qualities, giving an approach for obtaining different solid-state photoluminescence emitting materials by optimizing the inorganic framework or the decorating organic ligand. This is also the first report of photoluminescence phenomena in indium-phosphate systems. Extended studies are underway to reveal the synthetic requirements and explore their attractive properties.

(33) Nakayama, H.; Eguchi, T.; Nakamura, N.; Yamaguchi, S.; Danjyo, M.; Tsuhako, M. *J. Mater. Chem.* **1997**, *7*, 1063.
(34) Fan, R.; Zhu, D.; Mu, Y.; Li, G.; Yang, Y.; Su, Q.; Feng, S. *Eur. J. Inorg. Chem.* **2004**, 4891.
(35) Miller, D.; Swenson, D.; Gillan, E. *J. Am. Chem. Soc.* **2004**, *126*, 5372.

Acknowledgment. This work was supported by the Ministry of Science and Technology of China through the State Basic Research Project (G200077507) and the National Natural Science Foundation of China (20233030). The authors thank Dr. Jarrod F. Eubank for editing the English in the paper.

Supporting Information Available: Photographs of crystals, IR spectra, TGA curves, structure figures, and X-ray crystallographic data for **1**−**3**. This material is available free of charge via the Internet at http://pubs.acs.org.

CM052395X